Anharmonic interactions in beryllium oxide

G. Morell
College of General Studies, Department of Physical Sciences, University of Puerto Rico, San Juan, Puerto Rico 00931

W. Pérez, E. Ching-Prado, and R. S. Katiyar
Department of Physics, University of Puerto Rico, San Juan, Puerto Rico 00931-3343
(Received 28 December 1994; revised manuscript received 16 October 1995)

BeO is an insulator with an unusually high thermal conductivity (92% that of Cu at 25 °C) and a high Debye temperature (1280 K). We measured its first-order Raman scattering as a function of temperature from 300 down to 30 K. The temperature dependence of the energy and lifetime of its normal modes were analyzed in light of the theory of anharmonic phonon-phonon interactions, revealing that three-phonon up-conversion and down-conversion processes are present. We also measured the second-order Raman spectra of BeO, finding a number of bands that correspond well to previously reported second-order infrared-absorption measurements. In this way an old inconsistency was solved, since group theory predicts the infrared second-orders to be Raman-active as well, but they were never observed before. In addition, the thermal conductivity data of BeO were reexamined in order to explain their temperature dependence. We found that they have a quadratic dependence on the inverse absolute temperature after the conductivity maximum, all the way from 60 to 2000 K. Terms accounting for isotope and impurity scattering cannot be invoked in this material which is practically isotopically pure and with a low concentration of impurities. Umklapp interactions should be playing a dominant role, but the corresponding $\exp(\Theta_D/\alpha T)$ dependence is not observed. By taking into account the combined relaxation times of umklapp and normal processes it was possible to simulate these data, thus evidencing that the indirect effect of normal processes on thermal resistivity is significant and need to be taken into account.

I. INTRODUCTION

Beryllium oxide (also known as bromellite and beryllia) is a metal oxide ceramic that has found many applications due to its unusually high room-temperature thermal conductivity (3.7 W/cm K),[1] high electrical resistivity,[2] high bulk modulus (212 GPa, ranking among the hardest materials known),[3] high-energy gap (10.63 eV, direct),[4] and high melting point (2530 ± 10 °C).[5] It has been used as a nuclear moderator material[6] and as a chip carrier substrate[2] for high-power applications.

In addition, BeO has a number of anomalous properties which make it an interesting material from the physics point of view. It is the only alkaline-earth oxide crystallizing in the wurtzite structure, instead of the NaCl-type structure in which the other members of this family (MgO, CaO, SrO, and BaO) crystallize. X-ray measurements on BeO carried out at room temperature proved particularly difficult to analyze due to strong extinction effects, thus indicating the occurrence of relatively large anharmonic interactions.[7] The deviation in the u parameter is also related to the degree of crystal anharmonicity.[7] At room temperature, its c/a ratio is 1.623 and its internal parameter u is 0.3780.[8] The corresponding values for an ideal wurtzite structure are 1.633 and 0.3750, and for BeO the predicted u value is 0.3765.[8]

The wurtzite structure belongs to space group C_{6v}^4 ($P6_3mc$) with all atoms occupying C_{3v} sites.[7,9] Each Be atom is tetrahedrally coordinated to four O atoms and vice versa.[7] The number and symmetry of the optical modes at the zone center for C_{6v} are given by the representation[10]

$$\Gamma = A_1(z,z^2,x^2+y^2) + 2B_1 + E_1(x,y,xz,yz) + 2E_2(x^2-y^2,xy).$$

All modes are Raman active except B_1, which is silent. A_1 and E_1 are also polar. One can therefore observe both the longitudinal (LO) and transverse (TO) components of these modes in Raman spectroscopy by using the proper scattering geometry.[9,10] All Raman fundamentals of BeO have been measured and their polarization analyzed.[6,9,10] We observed three normal modes in the $z(xx)\bar{z}$ and $z(xy)\bar{z}$ scattering geometries at 338, 684, and 1082 cm^{-1} (room-temperature frequency values), in complete agreement with earlier reports.[6,9,10] Following previous assignments, these modes are the E_2^1, E_2^2, and A_1(LO) normal vibrational modes, respectively.[10] However, the band observed at around 1082 cm^{-1} in the $z(xy)\bar{z}$ scattering geometry is not pure A_1(LO), but a combination of E_1(LO) and A_1(LO).[10] Therefore it is a quasilongitudinal mode.

BeO has been the subject of an unsuccessful search for its predicted structural phase transition to the rocksalt structure.[11,12] Compounds crystallizing in the wurtzite structure can exhibit a structural phase transition to zinc blende and NaCl-type structures as a function of temperature and pressure.[13–16] The wurtzite-to-cubic structural phase transition in particular can be easily detected by the Raman technique since all first-order Raman scattering is forbidden in the NaCl-type structure. *Ab initio* pseudopotential calculations predicted a pressure-induced transition from wurtzite to a NaCl-type phase at about 20 GPa which could not be detected.[12] Later, calculations using the potential-induced

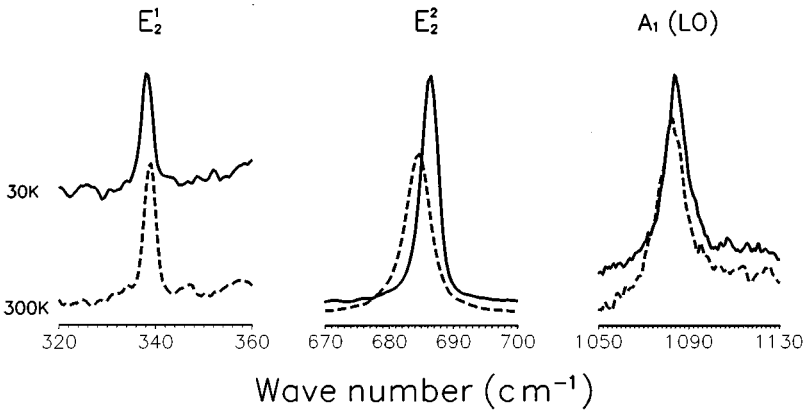

FIG. 1. Raman spectra of BeO taken in the $z(xx)\bar{z}$ scattering geometry at 30 and 300 K.

breathing (PIB) model predicted the same phase transition to occur at 40 GPa.[11] Raman experiments have shown BeO to remain in the wurtzite structure (and in the insulator state) at least up to 55 GPa.[11] Also, x-ray-diffraction experiments have not found this structural phase transition at high temperatures (298–1183 K),[3] and nor have Raman scattering experiments found it at low temperatures (35–293 K).[10]

BeO gives the seldom found opportunity of studying anharmonic phenomena below $0.25\Theta_D$ already at room temperature and down to $0.02\Theta_D$ using a liquid-He cryostat. This is because BeO has a high Debye temperature of 1280 K.[17] The temperature region down to $0.02\Theta_D$ contains information about the most elemental anharmonic interactions, and in most materials it falls below 10 K, being thus more difficult to study. However, no detailed study has been reported thus far on the effects of anharmonicity over the normal vibrational modes of BeO.

We investigated the anharmonic behavior of first-order Raman modes appearing in the $z(xx)\bar{z}$ and $z(xy)\bar{z}$ scattering geometries as a function of temperature in the interval from 30 to 300 K, collecting data at 20-K intervals. This allowed us to determine the relative contributions of down- and upconversions processes to the anharmonicity of the normal modes. In addition, we measured the second-order Raman spectra of BeO. This was possible thanks to charge coupled device (CCD) technology. In addition, the thermal conductivity data of BeO reported by Slack and Austerman[1] in 1971 were reexamined to explain their temperature dependence. This analysis provides additional information about the anharmonic phonon-phonon interactions in BeO.

II. EXPERIMENT

We obtained a highly transparent and flawless BeO single crystal of hexagonal shape and approximate dimensions 0.5 cm×0.3 cm×0.3 cm, through a collaboration with S. P. S. Porto.[9] This sample was mounted on the cold finger of a closed-cycle helium cryostat, from Cryogenic Technology, connected to a Lake Shore model DRC84C temperature controller. A platinum sensor placed near the sample was used to monitor the temperature. The 514.53-nm radiation line from a Coherent Innova 99 Ar-ion laser was used as the excitation source. The power impinging the sample was kept at 20 mW. A Jobin Yvon model S3000 triple monochromator configured in the subtractive mode and attached to a Raman microprobe was used to collect the Raman scattering. All the spectra were taken with a 20× objective that allows 15 mm of working distance and $\approx 5\times10^3$ μm^2 of illuminated area. A resolution of 1.9 cm^{-1} was used as measured from the width of the Ar-plasma lines. Light entered the sample along the crystallographic z axis polarized in the x direction. The scattering in the back direction was analyzed into x- or y-polarized components with respect to the crystal and measured using a 1024-channel diode array (Princeton Instruments). In order to correct for the grating efficiency dependence on polarization, a half-wave plate was placed in front of the spectrometer.

Any measured Raman line is the convolution of a triangular function, due to finite-slit effects, and a damped harmonic oscillator (DHO) function, multiplied by the thermal occupation factor $n(\omega,T)$. The triangular part can be approximated by a Gaussian function, so that after the data are divided by $n(\omega,T)$ we are left with a Voigt profile.[18] In the Voigt function there are two bandwidths to fit, one for the Gaussian and one for the damped harmonic oscillator contribution. The Gaussian part was obtained independently by measuring the half width (full width at half the maximum) of an argon-plasma line. This value was kept fixed in the equation of the Voigt profile, while the DHO center frequency, half width, and intensity were left as fitting parameters. Results obtained by assuming a triangular function are within 3% to those obtained by assuming a Gaussian function.[18] All the data were fitted using the Marquardt-Levenberg algorithm to find the absolute minimum of χ^2. Typical Raman spectra of BeO are shown in Fig. 1. The narrowest line is the lowest-energy one with an uncorrected half width around 2.5 cm^{-1}. This half width is beyond the experimental resolution of 1.9 cm^{-1}. Actual half widths obtained as explained above are smaller than the measured ones. They are the part that survives after removal of the instrumental width.

The second-order Raman scattering of BeO is extremely low so that we could only measure it by collecting data continuously for 20 min into a liquid-N-cooled (CCD ISA Spcetraview-2D). The intrinsic noise of this detector is less than one electron per pixel per hour. The sample was placed in the macrochamber of a model T64000 spectrometer from Instruments S.A. Laser radiation entered the sample through its crystallographic z direction. The scattered light was collected at right angles, in the x direction. A Coherent Ar-ion laser tuned at 514.53 nm provided the excitation ra-

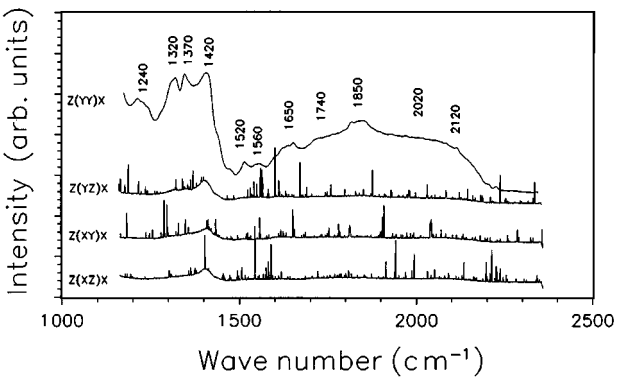

FIG. 2. Polarized second-order Raman spectra of BeO. The scattering geometry is indicated on the left side of each spectrum.

diation that impinged the sample at 70 mW. The incident light was polarized either along the y or x direction, while the scattered light was analyzed into its y or z components. We therefore had four different scattering geometries. The collected spectra turned out to be of very low intensity and shaped into broad overlapping bands, with many spikes due to cosmic rays reaching the CCD detector during the long collection time. Only the $z(yy)x$ spectrum was intense enough to afford cleaning up the spikes without distorting the bands. The other three spectra were left as measured. The second-order data are depicted in Fig. 2.

III. RESULTS AND DISCUSSION

A. Temperature dependent first-order Raman scattering

In general, the effect of an anharmonic potential over the lattice normal vibrational modes is to decrease their lifetime (broaden their width) and lower their energy (downshift their frequency) as temperature rises. These effects are seen to occur in the first-order Raman spectra of BeO shown in Fig. 1. We have studied the anharmonic behavior of the two E_2 modes and the A_1(LO) mode in detail. The observed (after the necessary corrections) half widths and frequencies as a function of temperature are plotted in Figs. 3, 4, and 7–10. We have simulated these data with well-known expressions derived from theoretical studies on the anharmonic oscillator.[18–25] Only those anharmonic terms which are linear in the occupation number (n_l) were considered since they provide the most important contributions in the temperature regime of interest.

The cubic contributions up to and including second-order terms are given by[24]

$$\Delta_l^{(2)} = -\frac{18}{\hbar^2}\sum_{mn}|B_{lmn}|^2\left(\frac{n_m+n_n+1}{\omega_l+\omega_m+\omega_n}-\frac{n_m+n_n+1}{\omega_l-\omega_m-\omega_n}+\frac{n_m-n_n}{\omega_l-\omega_m+\omega_n}-\frac{n_m-n_n}{\omega_l+\omega_m-\omega_n}\right)_P, \tag{1}$$

$$\Gamma_l^{(2)} = \frac{18\pi}{\hbar^2}\sum_{mn}|B_{lmn}|^2\{(n_m+n_n+1)[\delta(\omega_l-\omega_m-\omega_n) - \delta(\omega_l+\omega_m+\omega_n)]+(n_m-n_n)[\delta(\omega_l+\omega_m-\omega_n) - \delta(\omega_l-\omega_m+\omega_n)]\}, \tag{2}$$

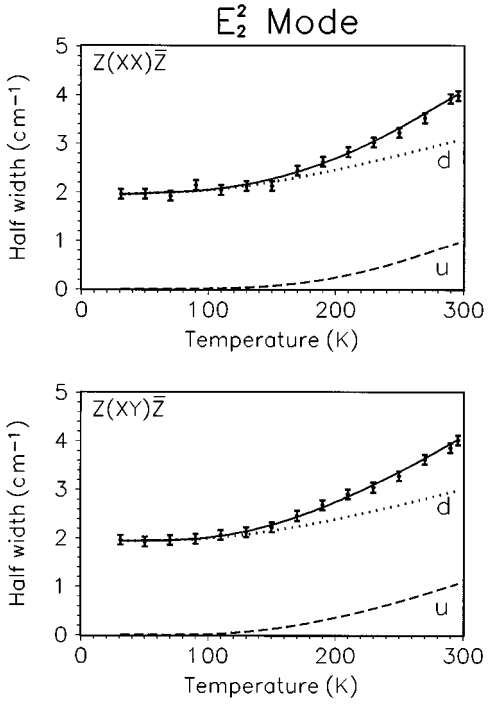

FIG. 3. Temperature dependence of the half width of the E_2^2 mode. The solid line is the fit to three-phonon anharmonic interactions. The contributions from down- and up-conversion processes are shown separately.

where the subscript P denotes the principal value. $\Delta^{(2)}$ and $\Gamma^{(2)}$ contain contributions from down-conversion (the first two terms) and up-conversion (the second two terms) three-phonon interactions. The contributions from up-conversion interactions vanish in the limit as T goes to zero, while down-conversion processes always have a finite contribution, even at 0 K. This contribution corresponds to the spontaneous decay of the given phonon into two lower-energy phonons, a process that always has a finite probability.[22]

The leading quartic term to second order corresponds to a process in which two phonons ω_l and ω_m of the thermal bath collide elastically, producing an anharmonic frequency shift on the optical phonon without changing its lifetime. This term is[22,25]

$$\Delta_l^{(2)} = \frac{12}{\hbar}B_{llm-m}(2n_m+1). \tag{3}$$

In order to obtain the complete expression for the frequency as a function of temperature, we must add the volume expansion contribution, the anharmonic contribution, and the zero-point frequency:[18,23]

$$\omega_l(T) = \omega_l^0 + \Delta_l^{\mathrm{vol}} + \Delta_l^{\mathrm{anh}}. \tag{4}$$

Thermal expansion is a manifestation of the lattice anharmonicity that has its own effects over the frequency, but none on the half width. The explicit form of the volume expansion contribution is[18,23]

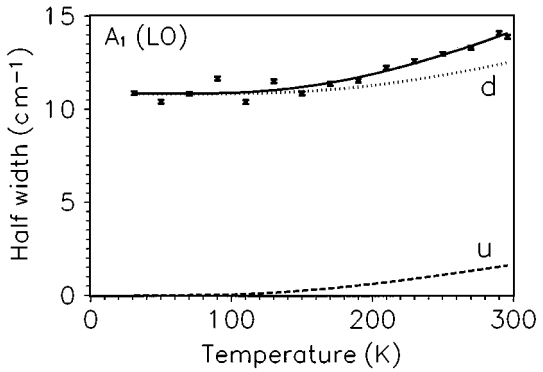

FIG. 4. Temperature dependence of the half width of the A_1(LO) mode. The solid line is the fit to three-phonon anharmonic interactions. The contributions from down- and up-conversion processes are shown separately.

$$\Delta_l^{\mathrm{vol}} = \omega_l^0 \left[\exp\left(\gamma_l \int_0^T \alpha_V dT \right) - 1 \right], \tag{5}$$

where γ is the mode Grüneisen parameter and α_v is the coefficient of volume expansion.

Three-phonon anharmonic interactions provide a satisfactory fit to the half width of the E_2^2 and A_1(LO) modes as shown by the solid lines in Figs. 3 and 4. These theoretical fits are decomposed into down-conversion (d) and up-conversion (u) contributions. It is readily noticed that up-conversion contributions become important only above 100 K, while down-conversion contributions are always present. These simulations were obtained by leaving the coefficients in front of the down- and up-conversion terms as adjustable parameters. Besides, we did not assume equipartition of energy among produced phonons or any requisite other than energy conservation. Therefore the frequencies of phonons created in the down-conversion processes and that of phonons participating in the up-conversion processes were

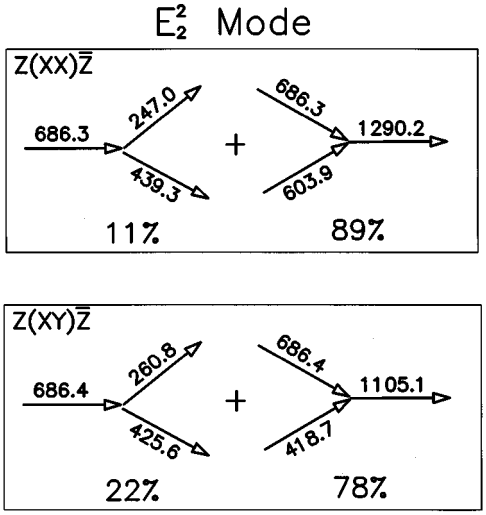

FIG. 5. Schematic representation of the numerical results obtained by simulating the half width of the E_2^2 mode to three phonon interactions. The percentages are the relative contributions from down- and up-conversion processes.

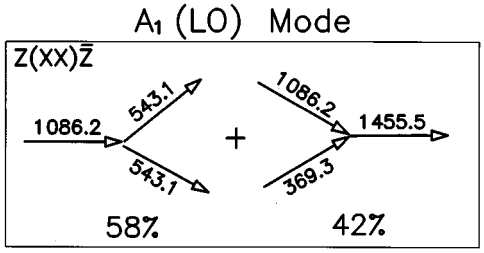

FIG. 6. Schematic representation of the numerical results obtained by simulating the half width of the A_1(LO) mode to three phonon interactions. The percentages are the relative contributions from down- and up-conversion processes.

left as adjustable parameters. Nevertheless, these frequencies only represent weighted averages or effective interaction paths since there are many interaction possibilities.[18] Although Raman scattering is probing only those phonons at the Brillouin zone center, interactions with all phonons across the Brillouin zone are allowed as long as they fulfill energy and momentum conservation.[18] The adjustable parameters corresponding to the coefficients of the two conversion processes give a measure of their relative probability.[26] They are expressed as percentages that maintain the ratio between the two parameters and represented diagramatically in Figs. 5 and 6, along with the frequency values obtained from the simulations. For the E_2^2 mode up-conversion processes have a high probability relative to down-conversion processes. This indicates an increased phonon density of states[26] at high frequencies around 1100 and 1300 cm^{-1}. In

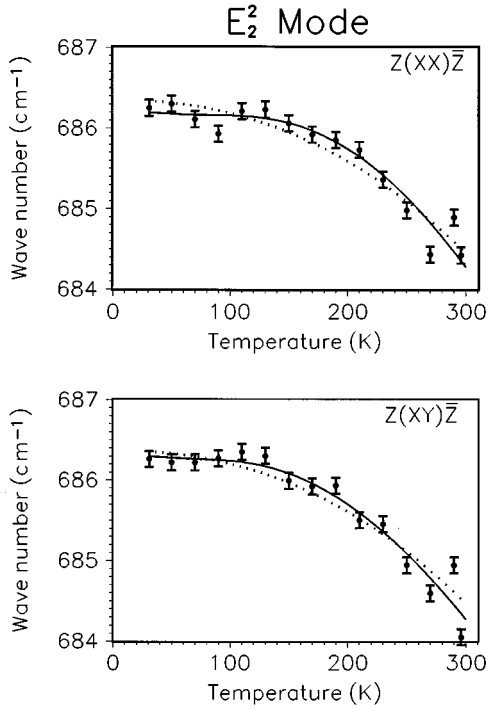

FIG. 7. Temperature dependence of the frequency of the E_2^2 mode. The dotted line is the fit to thermal expansion alone under the quasiharmonic approximation. The solid line is the fit having additional contributions from elastic scattering, down-conversion, and up-conversion processes.

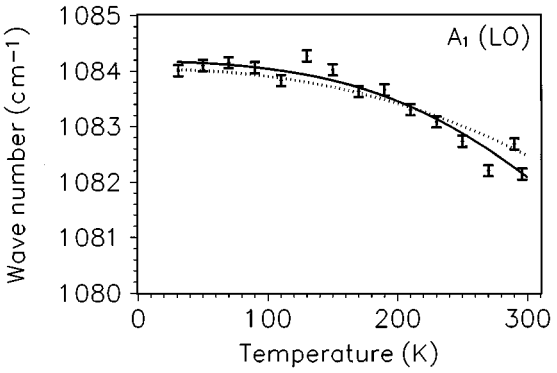

FIG. 8. Temperature dependence of the frequency of the A_1(LO) mode. The dotted line is the fit to thermal expansion alone under the quasiharmonic approximation. The solid line is the fit having additional contributions from elastic scattering, down-conversion, and up-conversion processes.

fact, the A_1(LO) mode falls in this region. This result is consistent with the fact that up-conversion processes start becoming important already at 100 K, a temperature at which the population of phonons with frequencies near 600 cm^{-1} needed for this up-conversion process is very small (less than 0.02%). This information about the phonon density of states (PDOS) of BeO is particularly relevant since there is no complete experimental PDOS available (only a few branches have been measured[27–29]) or any reliable theoretical PDOS of BeO (all attempts to satisfactorily reproduce the incomplete experimental data have failed[30–33]). These characteristics of the PDOS indicated by the anharmonicity of the normal modes should be obtained by any calculation of the vibrational branches and the corresponding PDOS of BeO.

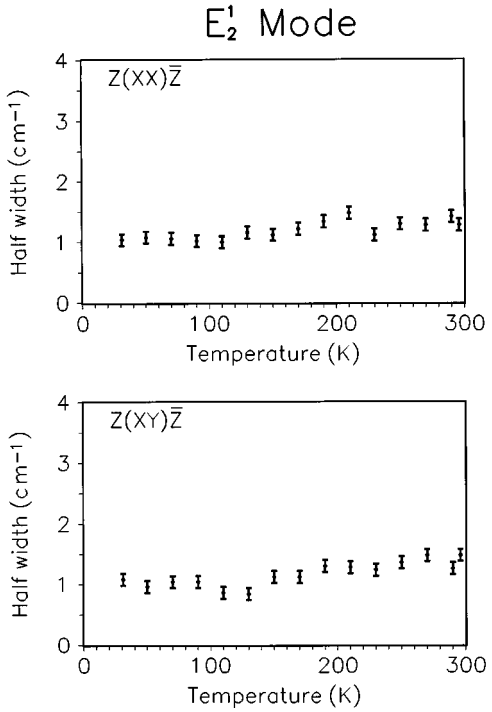

FIG. 9. Temperature dependence of the half width of the E_2^1 mode.

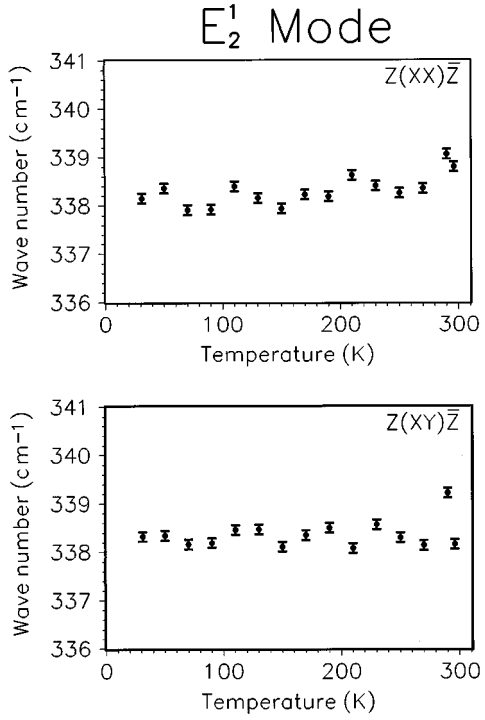

FIG. 10. Temperature dependence of the frequency of the E_2^1 mode.

Turning now to the fitted parameters of the A_1(LO) mode, we see (Fig. 6) a different picture. For this mode down-conversion processes dominate slightly in terms of their probability. This is consistent with the fact that the A_1(LO) mode is at the high-frequency edge of the PDOS. It can either become down converted, producing two first-order phonons, or combine with another phonon, giving rise to a second-order vibrational mode. Although down-conversion interactions dominate, second orders are indeed produced and we observed them. Notice also that for the down-conversion process equipartition of energy was obtained as the best fitted parameter without assuming it. Running this simulation with many different initial values always finished in the same result, indicating that this effective interaction path is not a mathematical artifact.

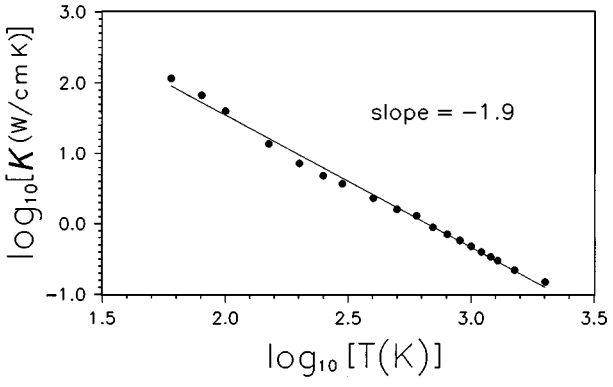

FIG. 11. Thermal conductivity of BeO plotted in a log-log plane. A straight line is obtained with a slope ≈ -2. This plot illustrates that κ is a power law of the inverse absolute temperature.

TABLE I. Numerical data obtained from the simulation of the frequency of the E_2^2 and A_1 (LO) modes. ω^0 is the zero-point frequency, ω' is the effective frequency of the phonons interacting elastically with ω^0, and χ^2 is an statistical parameter measuring the goodness of fit.

Normal mode (polarization)	ω^0 (cm^{-1})	ω' (cm^{-1})	χ^2 (thermal expansion term only)	χ^2 (including all terms)
E_2^2 (XX)	686.35	213.84	0.5508	0.4693
E_2^2 (XY)	686.36	219.43	0.6365	0.4713
A_1 (LO)	1084.04	415.69	1.0186	0.5809

Normal mode frequencies have an important contribution from the lattice thermal expansion that cannot be neglected. In fact, thermal expansion alone simulates the experimental data quite well (dotted lines in Figs. 7 and 8). To calculate this term we needed $\alpha_v(T)$ in Eq. (5), which was obtained by fitting the thermal expansion data of Sirota *et al.*[34] to a polynomial: $\alpha_v = 2.308\times10^{-8}T + 4.830\times10^{-11}T^2$. Mode Grüneisen parameters are also available:[11] 0.04 for E_2^1, 1.88 for E_2^2, and 0.98 for A_1(LO). The only adjustable parameter is ω^0. These simulations are improved to a certain extent when down- and up-conversion cubic terms [Eq. (1)] are included together with the pure elastic scattering quartic term [Eq. (3)]. The reason is that the two cubic terms have the effect of decreasing the frequency as the temperature increases, while the quartic term considered here has the opposite effect. Therefore they tend to cancel one another, allowing the thermal expansion to operate on the normal mode frequencies with minor adjustments. Statistical data comparing the goodness of fit with and without cubic and quartic terms are shown in Table I. The fitting parameter corresponding to the effective frequency ω' for elastic scattering with each given vibrational mode is also given in this table.

We have left the analysis of the E_2^1 mode for the end. The half width and frequency of this mode behave practically harmonic. Fluctuations observed in Figs. 9 and 10 show no particular trend and most of them are within the experimental uncertainty. Besides, the mode Grüneisen parameter of E_2^1 is virtually zero,[11] meaning that it remains insensitive to volume changes. A similar behavior was found in the E_2^1 mode of AgI, another wurtzite material. In AgI, E_2^1 remains constant even across structural phase transitions.[15,35] The E_2^1 mode average frequency is 338.3 ± 0.3 cm^{-1}, and its average half width is 1.2 ± 0.2 cm^{-1}. Together, these experimental results indicate that the E_2^1 mode is harmonic or nearly so, i.e., that its potential energy is quadratic in the interatomic displacements. This is a fine example of a normal vibrational mode showing simple harmonic behavior.

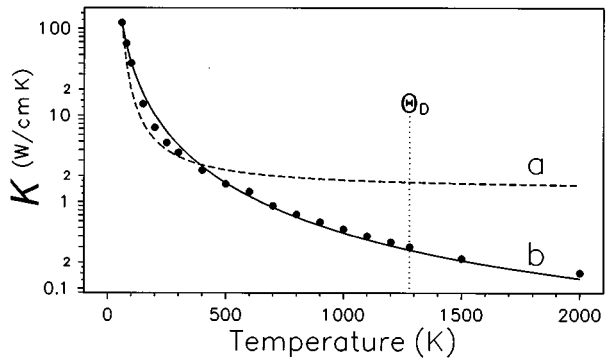

FIG. 12. Thermal conductivity of BeO (dots) from Slack (Ref. 1). Curve *a* is the best fit to the expression $\kappa \propto \exp(\Theta/\alpha T) + 1/T$, which takes into account umklapp resistance alone. Curve *b* is the best fit to T^{-2} as predicted by a model that takes into account normal processes (Ref. 38).

B. Second-order Raman scattering

It is not difficult to foresee that many materials will be restudied by detecting their Raman scattering onto a CCD, looking for features that photomultipliers and diode arrays might have left undiscovered. Previous researchers reported the Raman spectra of BeO to be ''clean'' above 1100 cm^{-1}.[6,9] Infrared spectroscopy was, however, able to detect second-order vibrational modes.[6] Here is where a serious inconsistency existed until our measurements. According to group theory, all infrared-active modes are also Raman active. A second-order mode can be infrared active only if the reduced representation of the product of the two (or more) modes that are combining contains at least one infrared-active species.[36] In wurtzite (C_{6v}) materials, this condition automatically guaranties that all infrared-active second orders are also Raman active. In fact, two of us had unsuccessfully searched for the second-order Raman spectra of BeO before utilizing both a photomultiplier and a diode-array detector.[10] In addition to the infrared second-order spectra, our analysis of the anharmonic behavior of the A_1(LO) mode indicated that second orders should be present.

The second-order Raman spectra of BeO are shown in Fig. 2. Four different polarization geometries were employed, but only the yy-polarized spectrum shows well-defined features up to 2400 cm^{-1}. The positions of bands and shoulders are annotated on top. They generally agree with the infrared measurements of Loh,[6] especially when taking into account the broad nature of second-order scattering. We did not, however, observe features at around 3000 cm^{-1} corresponding to four-phonon interactions. If present, these signals would be too weak to be detected. The second-order infrared band frequencies observed by Loh[6] are compared with our Raman measurements in Table II.

C. Thermal conductivity

The thermal conductivity of BeO was measured by Slack and Austerman[1] in 1971, using large single crystals. They joined their low-temperature data with that measured on ceramic samples at higher temperatures, passing through the Debye temperature at 1280 K, up to 2000 K. The interpretation of these data remained, in our point of view, incomplete. This is especially true for the values between the conductivity maximum at 45 K and the Debye temperature, for which they show that BeO behaves significantly different to other isotopically clean dielectrics like Al_2O_3, CaF_2, and NaF, in reduced coordinates (see Fig. 3 of Ref. 1). The interpretation of the thermal conductivity of dielectrics provides informa-

TABLE II. Comparison of the second-order band frequencies found by Raman (this work) and by infrared (Ref. 6) spectroscopies.

Raman second order (cm^{-1})	Infrared second order (cm^{-1})[a]
	1200
1240	1220
	1286
1320	1317
	1340
1370	1374
1420	1400
1520	1540
1560	1569
	1596
1650	
1740	1720
1850	
2020	2019
	2046
2120	2100
	2215
	2400
	2579
	2730
	2910
	3333

[a]Reference 6.

tion about the phonon-phonon interactions of acoustic modes which complements that obtained from Raman scattering about the optical modes.

The major impurity found in BeO single crystal was Al with 130 ppm.[1] All other impurity concentrations are much lower. Therefore impurity scattering can be neglected. Besides, BeO is practically isotopically pure.[1] Be has only one natural isotope, Be^9, and natural oxygen is 99.8% O^{16}. So point-defect scattering can also be neglected. The boundary scattering regime is situated below 10 K,[1] where the conductivity is proportional to T^3. We are thus left with umklapp and normal processes to account for the observed decrease in thermal conductivity after the conductivity maximum at 45 K.

A log-log plot of the thermal conductivity data yields a straight line with a slope of ≈ -2 (see Fig. 11). This is a clear indication that a power law in the inverse absolute temperature is operating. If we are to consider umklapp processes as the only source of heat resistivity, an exponential law would be expected:[37]

$$\kappa \propto \exp\left(\frac{\Theta_D}{\alpha T}\right). \tag{6}$$

Curve *a* in Fig. 12 is the best simulation to this expression with the preexponential coefficient and factor *a* as fitting parameters. It can be concluded at once that a more complex mechanism must be operating. Callaway[38] developed a model for lattice thermal conductivity that takes into account the relaxation times of both normal and umklapp processes. Although normal processes do not produce heat resistivity directly, they can enhance the effectivity of umklapp processes by working to restore the equilibrium populations of phonons depleted during umklapp interactions. Callaway's[38] model predicts that in the case of isotopically pure wurtzite dielectric materials the thermal conductivity varies as T^{-2} beyond the low-temperature conductivity maximum. BeO is a material that fulfills to a great extent the conditions of the model, and its behavior is very close to the model's prediction. Curve *b* in Fig. 12 is the simulation of the thermal conductivity to T^{-2}:

$$\kappa = (4\times 10^5) T^{-2}. \tag{7}$$

This expression is found to satisfactorily fit the experimental data all the way from 45 to 2000 K. Above $\Theta_D = 1280$ K, quartic anharmonic interactions should be playing some role. Since quartic terms[39] also vary as T^{-2}, it is not possible to separate their contribution.

IV. CONCLUSIONS

We have studied the temperature dependence of the first-order Raman scattering of BeO from 300 down to 30 K. The experimental data corresponding to the E_2^2 and the A_1(LO) modes were found to be satisfactorily explained within the theory of anharmonic interactions that takes into account cubic anharmonic terms to second order and the leading quartic anharmonic term, that is, terms which contain the phonon occupation number to the first power. Corrections to volume expansion effects were also taken into account within the quasiharmonic theory. Down-conversion processes were found to dominate the interactions of the E_2^2 and the A_1(LO) modes. At the same time, the fact that up-conversion processes have a noticeable effect beginning at 100 K indicated a high phonon density of states at frequencies above 1000 cm^{-1}. The lowest-frequency mode E_2^1 was observed to remain practically unchanged in its half width and frequency, indicating a harmonic behavior.

We also measured the second-order Raman spectra of BeO. Group theoretical results predict that for wurtzite materials all vibrational modes, first or second order, which are infrared active must also be Raman active.

In addition, we analyzed the thermal conductivity data of BeO from Slack and Austerman[1] in light of a model developed by Callaway[38] for the lattice thermal conductivity in isotopically pure materials. This model takes into account the indirect role of normal processes in producing heat resistivity. BeO is an example of a material in which only intrinsic phonon-phonon thermal resistivity processes need to be considered, thus giving the opportunity of testing Callaway's[38] model. We found that the thermal conductivity data follow the predicted T^{-2} dependence. The equation of the umklapp processes alone, on the other hand, did not give a satisfactory fit, making it evident that the indirect role of normal processes in the thermal resistivity is significant and needs to be taken into account when calculating the intrinsic lattice thermal conductivity.

ACKNOWLEDGMENTS

We want to gratefully acknowledge the insightful discussions held with Dr. Manuel Cardona while he recently visited the University of Puerto Rico. This work was supported by EPSCoR-NSF Grant No. EHR-9108775.

[1] G. A. Slack and S. B. Austerman, J. Appl. Phys. **42**, 4713 (1971).
[2] S. S. Shinozaki, J. Hangas, and K. Maeda, in *Electronic Packaging Materials Science III*, edited by R. Jaccodine, K. A. Jackson, and R. C. Sundahl, MRS Symposia Proceedings No. 108 (Materials Research Society, Pittsburgh, 1988), p. 89.
[3] R. M. Hazen and L. W. Finger, J. Appl. Phys. **59**, 3728 (1986).
[4] D. M. Roessler, W. C. Walker, and E. Loh, J. Phys. Chem. Solids **30**, 157 (1969).
[5] *Handbook of Chemistry and Physics*, 67th ed. edited by R. C. Weast (CRC Press, West Palm Beach, FL, 1986).
[6] E. Loh, Phys. Rev. **166**, 673 (1968).
[7] G. Vidal-Valat, J. P. Vidal, K. Kurki-Suonio, and R. Kurki-Suonio, Acta Crystallogr. A **43**, 540 (1987).
[8] S. L. Mair and Z. Barnea, Acta Crystallogr. A **31**, 201 (1975).
[9] C. A. Arguello, D. L. Rousseau, and S. P. S. Porto, Phys. Rev. **181**, 1351 (1969).
[10] S. Devanarayanan, G. Morell, and R. S. Katiyar, J. Raman Spectrosc. **22**, 311 (1991).
[11] A. P. Jephcoat, R. J. Hemley, H. K. Mao, R. E. Cohen, and M. J. Mehl, Phys. Rev. B **37**, 4727 (1988).
[12] G. A. Kourouklis, A. K. Sood, and H. D. Hochheimer, Phys. Rev. B **31**, 8332 (1985).
[13] P. E. Van Camp, V. E. Van Doren, and J. T. Devreese, Phys. Rev. B **44**, 9056 (1991).
[14] K. J. Chang and M. L. Cohen, Solid State Commun. **50** 487 (1984).
[15] W. Bührer and P. Brüesch, Solid State Commun. **16**, 155 (1975).
[16] E. Chang and G. R. Barsch, J. Phys. Chem. Solids **34**, 1543 (1973).
[17] C. F. Cline, H. L. Dunegan, and G. W. Henderson, J. Appl. Phys. **38**, 1944 (1967).
[18] J. Menéndez and M. Cardona, Phys. Rev. B **29**, 2051 (1984).
[19] A. A. Maradudin and A. E. Fein, Phys. Rev. **128**, 2589 (1962).
[20] R. A. Cowley, Proc. Phys. Soc. London **84**, 281 (1964).
[21] I. P. Ipatova, A. A. Maradudin, and R. F. Wallis, Phys. Rev. **155**, 882 (1967).
[22] S. Califano, V. Schettino, and N. Neto, *Lattice Dynamics of Molecular Crystals*, Lecture Notes in Chemistry Vol. 26 (Springer, Berlin, 1981); S. Califano and V. Schettino, Int. Rev. Phys. Chem. **7**, 19 (1988).
[23] T. Sakurai and T. Sato, Phys. Rev. B **4**, 583 (1971).
[24] M. Balkanski, R. F. Wallis, and E. Haro, Phys. Rev. B **28**, 1928 (1983).
[25] R. F. Wallis, I. P. Ipatova, and A. A. Maradudin, Sov. Phys. Solid State **8**, 850 (1966).
[26] J. C. Bellows and P. N. Prasad, J. Chem. Phys. **70**, 1864 (1979).
[27] R. M. Brugger, K. A. Strong, and J. M. Carpenter, J. Phys. Chem. Solids **28**, 249 (1967).
[28] G. L. Ostheller, R. E. Schmunk, R. M. Brugger, and R. J. Kearnly, *Inelastic Neutron Scattering* (IAEA, Vienna, 1968), Vol. 1, p. 315.
[29] R. N. Sinclair (unpublished).
[30] A. W. Hewat, Solid State Commun. **8**, 187 (1970).
[31] R. Ramani, K. K. Mani, and R. P. Singh, Phys. Rev. B **14**, 2659 (1976).
[32] N. Rani, D. K. Gupta, and H. C. Gupta, Indian J. Pure Appl. Phys. **19**, 316 (1981).
[33] S. V. Danilov, A. V. Kruzhalov, V. G. Mazurenko, V. A. Maslov, and V. I. Surikov, Sov. Phys. Solid State **22**, 1854 (1980).
[34] N. N. Sirota, A. M. Kuz'mina, and L. P. Poluchankina, Sov. Phys. Dokl. **32**, 604 (1987).
[35] W. Bührer, R. M. Nicklow, and P. Brüesch, Phys. Rev. B **17**, 3362 (1978).
[36] A. Anderson, *The Raman Effect* (Dekker, New York, 1971), Vol. I, p. 118.
[37] Y. J. Han and P. G. Klemens, Phys. Rev. B **48**, 6033 (1993).
[38] J. Callaway, Phys. Rev. **113**, 1046 (1959).
[39] Y. P. Joshi, M. D. Tiwari, and G. S. Verma, Phys. Rev. B **1**, 642 (1970).